Endothelial tip/stalk cell selection requires BMP9-induced β_{IV}-spectrin expression during sprouting angiogenesis

Tasmia Ahmed[a,†], Aaron Ramonett[b,†], Eun-A Kwak[b], Sanjay Kumar[c], Paola Cruz Flores[a], Hannah R. Ortiz[b], Paul R. Langlais[d], Thomas J. Hund[e], Karthikeyan Mythreye[f,*], and Nam Y. Lee[a,b,g,*]

[a]Department of Chemistry & Biochemistry, [b]Department of Pharmacology, [d]Department of Medicine, and [g]Comprehensive Cancer Center, University of Arizona, Tucson, AZ 85724; [c]Division of Biology, Indian Institute of Science Education and Research, Tirupati 517507, India; [e]Department of Biomedical Engineering, Ohio State University, Columbus, OH 43210; [f]Department of Pathology, University of Alabama at Birmingham, Birmingham, AL 35294

ABSTRACT **β_{IV}-Spectrin is a membrane cytoskeletal protein with specialized roles in the nervous system and heart. Recent evidence also indicates a fundamental role for β_{IV}-spectrin in angiogenesis as its endothelial-specific gene deletion in mice enhances embryonic lethality due to hypervascularization and hemorrhagic defects. During early vascular sprouting, β_{IV}-spectrin is believed to inhibit tip cell sprouting in favor of the stalk cell phenotype by mediating VEGFR2 internalization and degradation. Despite these essential roles, mechanisms governing β_{IV}-spectrin expression remain unknown. Here we identify bone morphogenetic protein 9 (BMP9) as a major inducer of β_{IV}-spectrin gene expression in the vascular system. We show that BMP9 signals through the ALK1/Smad1 pathway to induce β_{IV}-spectrin expression, which then recruits CaMKII to the cell membrane to induce phosphorylation-dependent VEGFR2 turnover. Although BMP9 signaling promotes stalk cell behavior through activation of hallmark stalk cell genes ID-1/3 and Hes-1 and Notch signaling cross-talk, we find that β_{IV}-spectrin acts upstream of these pathways as loss of β_{IV}-spectrin in neonate mice leads to retinal hypervascularization due to excessive VEGFR2 levels, increased tip cell populations, and strong Notch inhibition irrespective of BMP9 treatment. These findings demonstrate β_{IV}-spectrin as a BMP9 gene target critical for tip/stalk cell selection during nascent vessel sprouting.**

Monitoring Editor
Terry Lechler
Duke University

Received: Feb 23, 2023
Revised: Apr 14, 2023
Accepted: Apr 19, 2023

This article was published online ahead of print in MBoC in Press (http://www.molbiolcell.org/cgi/doi/10.1091/mbc.E23-02-0064) on April 26, 2023.

†These authors contributed equally to the work.

Conflict of interest: The authors declare no conflict of interests.

Author contributions: T.A., A.R., E-A.K., and S.K. conducted the majority of the experiments and analysis; P.C.F. and H.R.O. contributed to data analysis. P.R.L. assisted with all MS proteomics work and data analysis. T.J.H. assisted with the writing of the manuscript. N.Y.L. and K.M. conceived the study, analyzed all data, and prepared and edited the manuscript.

*Address correspondence to: Nam Y. Lee (namlee@email.arizona.edu); Karthikeyan Mythreye (mkarthikeyan@uabmc.edu).

Abbreviations used: BMP9, bone morphogenetic protein 9; EC, endothelial cell; ALK1, activin receptor–like kinase-1.

INTRODUCTION

Spectrins are membrane cytoskeletal proteins that maintain cell shape and structural support of many integral membrane proteins (Cianci *et al*., 1999; Djinovic-Carugo *et al*., 2002; Machnicka *et al*., 2014). The two α subunits and five β subunits found in the mammalian system exist as heterotetramers to coordinate diverse cellular functions, such as cell adhesion, signaling, and mechanotransduction (Berghs *et al*., 2000; Bennett and Baines, 2001; Bennett and Lorenzo, 2013, 2016). Mutations in spectrins have been linked to many human diseases, including congenital myopathy, neuropathy, and hemolytic anemia (Gaetani *et al*., 2008; Knierim *et al*., 2017; Gallagher *et al*., 2019; Liu and Rasband, 2019). But while most spectrin subunits are broadly expressed, β_{IV}-spectrin appears to be more specialized, so far being characterized only in the nervous system, heart, pancreatic β-cells (Yang *et al*., 2007; Hund *et al*., 2010; Kline *et al*., 2013), and recently by our group, in vascular endothelial cells (ECs) (Kwak *et al*., 2022).

We initially discovered β_{IV}-spectrin as a new EC marker during proteomic profiling of proteins associated with angiogenesis and subsequently determined its novel role in angiogenesis and vascular patterning in vivo (Kwak *et al.*, 2022). By generating an inducible EC-specific gene deletion mouse model, we showed that early loss of β_{IV}-spectrin promotes embryonic lethality due to hypervascularization and hemorrhagic defects, whereas in the neonatal retina, β_{IV}-spectrin depletion causes a striking increase in vascular density and tip cell populations (Kwak *et al.*, 2022). We subsequently found that β_{IV}-spectrin enhances VEGFR2 turnover by recruiting CaMKII to the plasma membrane, which in turn phosphorylates VEGFR2 at Ser-984, a previously uncharacterized phosphoregulatory site that critically induces VEGFR2 internalization and degradation (Kwak *et al.*, 2022).

But while this phosphorylation-dependent VEGFR2 turnover strongly inhibits the tip cell potential in nascent sprouting vessels, we further observed that β_{IV}-spectrin is selectively expressed in stalk cells but not tip cells of sprouting vessels and is largely absent in quiescent vessels, indicating that β_{IV}-spectrin is spatiotemporally regulated (Kwak *et al.*, 2022). And given that mechanisms regulating β_{IV}-spectrin levels remain unknown in any tissue type, we sought to identify the first molecular pathways governing its dynamic expression. Here, we report bone morphogenetic protein 9 (BMP9) as a potent inducer of gene expression that proves critical for the proper maintenance of tip/stalk cell dynamics during sprouting angiogenesis and vascular patterning.

RESULTS

BMP9 is a strong inducer of β_{IV}-spectrin expression in nascent vessels

On the basis of the recent identification of β_{IV}-spectrin as an endothelial marker predominantly expressed in active sprouting vessels (Kwak *et al.*, 2022), in the present study we performed a ligand screen to determine which angiogenic factors might induce its expression. Preliminary Western analysis of β_{IV}-spectrin expression in mouse embryonic ECs (MEECs) showed that, among a diverse group of ligands tested, only BMP9, a circulating vascular quiescence factor (David *et al.*, 2008; Desroches-Castan *et al.*, 2022), strongly induced β_{IV}-spectrin expression over basal levels (Figure 1A). Consistent with the biochemical results, immunofluorescence imaging revealed a robust BMP9-dependent increase in β_{IV}-spectrin along the basolateral membrane regions (Figure 1B), thus corroborating our previous observation that β_{IV}-spectrin localizes mostly to the basolateral compartments of actively proliferating ECs (Kwak *et al.*, 2022). Importantly, this effect was evidenced in vivo, where BMP9 treatment via intraperitoneal (IP) injection resulted in a more than threefold increase in β_{IV}-spectrin expression along the sprouting vascular plexus of the newborn mouse retina (Figure 1C).

BMP9 regulation of angiogenesis requires β_{IV}-spectrin expression

BMPs were originally identified as inducers of bone growth and cartilage formation (Urist, 1965; Wozney *et al.*, 1988) but have since been shown to regulate cell growth, differentiation, and survival of various cell types (Hemmati Brivanlou and Thomsen, 1995; Kobayashi *et al.*, 2005; Stewart *et al.*, 2010; Wang *et al.*, 2014). In the case of BMP9, there is mounting evidence that it acts as a potent vascular quiescence factor (Scharpfenecker *et al.*, 2007; David *et al.*, 2008; Larrivée *et al.*, 2012; Ricard *et al.*, 2012; Ruiz *et al.*, 2016, 2020; Desroches-Castan *et al.*, 2022). Indeed, several independent studies have now shown that neutralizing this liver-derived circulating factor with antibodies or ligand traps causes hypervascularization and arteriovenous malformations, whereas ectopic BMP9 treatment inhibits vascular sprouting (Scharpfenecker *et al.*, 2007; Larrivée *et al.*, 2012; Ricard *et al.*, 2012; Ruiz *et al.*, 2016, 2020). While the underlying mechanisms are not fully resolved, we tested whether BMP9 could either suppress or normalize the prominent hypersprouting defect typically observed in our endothelial-specific β_{IV}-spectrin knockout (β_{IV}-EC^{KO}) mice (Kwak *et al.*, 2022). To do so, tamoxifen was first administered to β_{IV}-EC^{KO} newborn mice at postnatal day 1 (P1) and P3 to induce the gene knockout along with treatment with or without BMP9 via IP injection. Neonate retinas were then isolated at P5 followed by fluorescence staining with isolectin B4 (IB4) (Figure 2). Consistent with previous findings, BMP9 treatment in neonate mice reduced the overall number of branched capillary networks compared with control (Figure 2A, graph), whereas the β_{IV}-EC^{KO} neonate retina displayed excessive vascular density irrespective of the ligand treatment (Figure 2B, graph), suggesting that BMP9 suppression of sprouting angiogenesis strictly requires β_{IV}-spectrin expression.

β_{IV}-Spectrin gene expression is mediated by the BMP9/ALK1/Smad1/5 pathway

BMP9 is a high-affinity ligand for the activin receptor–like kinase-1 (ALK1), an EC-specific type I receptor that phosphorylates and activates downstream Smad1/5 transcriptional effectors (David *et al.*, 2007; Scharpfenecker *et al.*, 2007; Larrivée *et al.*, 2012; Ricard *et al.*, 2012). We therefore tested whether β_{IV}-spectrin is a novel gene target downstream of the BMP9/ALK1/Smad1/5 pathway by performing real time quantitative PCR (RT-qPCR). Here, we observed at least a threefold induction in β_{IV}-spectrin transcript levels in response to BMP9 compared with the basal state and to other ligands, indicating that BMP9 selectively enhances its gene expression (Figure 3A). To further test whether this transcriptional activation requires ALK1, we performed a parallel experiment where cells were pretreated with LDN193189, a small-molecule inhibitor of the ALK1 kinase (Yu *et al.*, 2008). The kinase inhibitor effectively suppressed the BMP9 responsiveness even at submicromolar concentrations over the course of 12–18 h relative to the stable β_{IV}-spectrin–depleted ECs serving as negative control (Figure 3B). Next, we confirmed that BMP9 signals specifically through the canonical Smad1 pathway by assessing for BMP9-induced β_{IV}-spectrin expression in stable Smad1-knockdown ECs (Supplemental Figure S1). Here, BMP9 treatment strongly induced β_{IV}-spectrin expression in an ALK1 kinase–dependent manner in control but not in Smad1-depleted cells (Figure 3C, graph), thus indicating that β_{IV}-spectrin is a newly identified gene target of the BMP9/ALK1/Smad1 pathway in ECs (Figure 3D).

β_{IV}-Spectrin is required for BMP9-dependent enhancement of the stalk cell phenotype

BMP9 is considered a powerful enhancer of the stalk cell phenotype during sprouting angiogenesis as it directly and indirectly up-regulates multiple stalk cell–associated genes (Moya *et al.*, 2012; Rostama *et al.*, 2015; Tillet and Bailly, 2015; Guihard *et al.*, 2020; Seong *et al.*, 2021). Accordingly, we sought to determine what role the BMP9-induced β_{IV}-spectrin expression plays in the tip/stalk cell selection process in vivo. As expected, BMP9 treatment in control mice resulted in a significant reduction in tip cells, as evidenced by both the overall decrease in CD34 staining (green) along the leading edge of the vascular front and fewer filopodial projections (Supplemental Figure S2 and Figure 4A; white arrows). This marked suppression in tip cell potential was inversely proportional with the enhanced β_{IV}-spectrin expression (red) in the trailing stalk cell populations of sprouting retinal vessels (Supplemental Figure S2 and

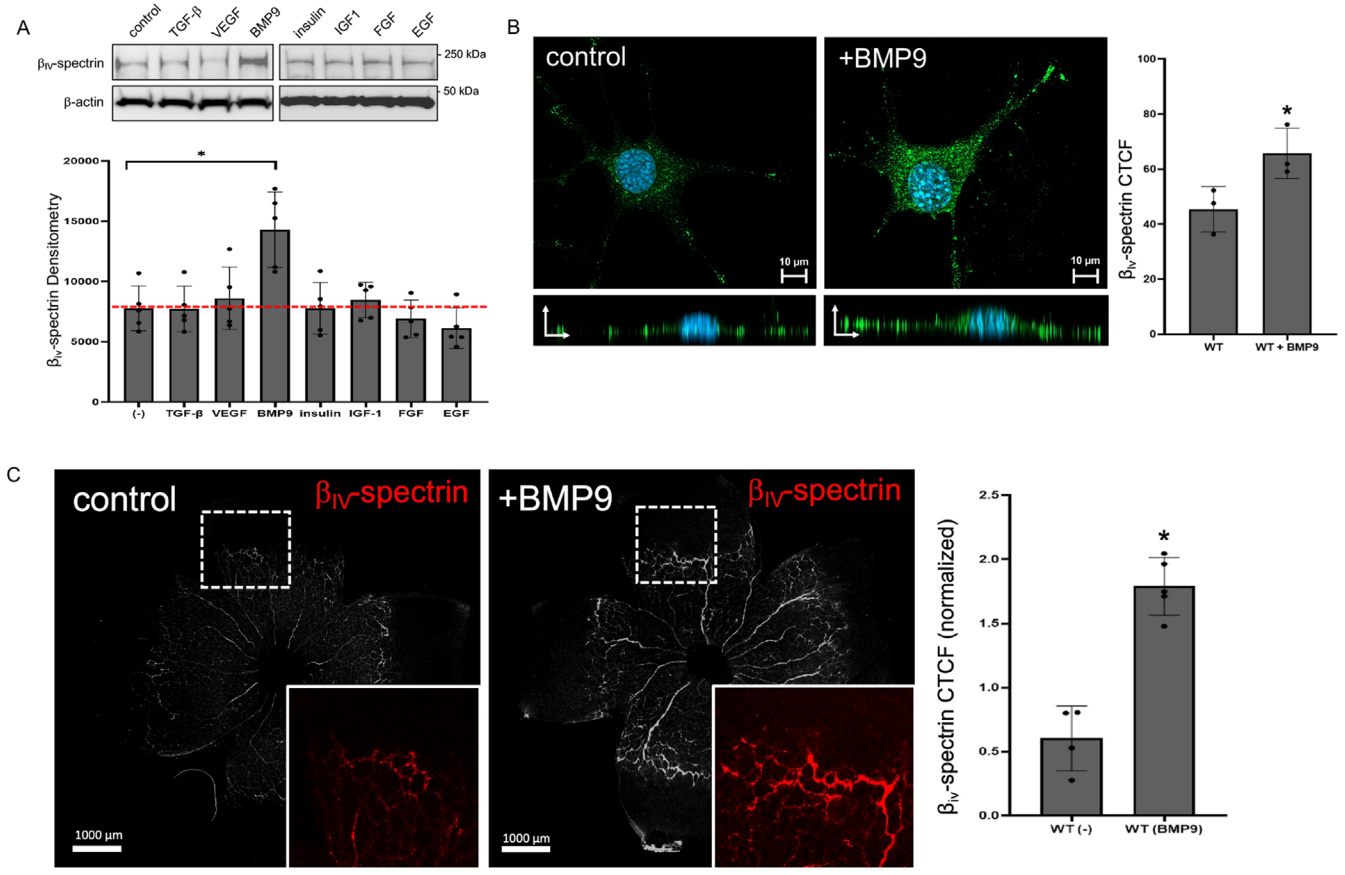

FIGURE 1: BMP9 induces β_{IV}-spectrin expression in ECs and nascent retinal vessels. (A) Western blot and densitometry quantifications show relative endogenous β_{IV}-spectrin expression in MEECs cultured in serum-deprived media supplemented with TGF-β1 (200 pM), VEGF (50 ng/ml), BMP9 (1 nM), insulin (100 nM), IGF-1 (200 nM), FGF (10 ng/ml), or EGF (10 ng/ml) for 16 h. Error bars indicate mean with standard deviation (SD), and the type 2 *t* test result shows $*p <$ 0.005 relative to control (no treatment) based on three independent experiments. (B) Representative immunofluorescence images show β_{IV}-spectrin staining in MEECs upon BMP9 (1 nM) treatment in serum-starved condition for 16 h. Graph represents average VEGFR2 fluorescence as quantified by CTCF (corrected total cell fluorescence). Fifty cells were analyzed per group from three independent experiments. Error bars indicate mean with SD, and the type 2 *t* test result shows $*p < 0.05$ relative to control (PBS). (C) Representative immunofluorescence images show β_{IV}-spectrin staining in P5 wild-type (WT) retina upon BMP9 treatment (1 nM) via IP injection at P1 and P3. Graph quantification is based on average normalized CTCF values from five separate mice for both WT control and WT BMP9-treated retinas. Error bars indicate mean with SD, and the type 2 *t* test result shows $*p < 0.03$ relative to control (PBS).

Figure 4A; graphs). In β_{IV}-EC^{KO} postnatal mice, however, the overall CD34 levels and filopodial counts remained dramatically elevated independent of BMP9 (Figure 4A, graph). As these results demonstrated that BMP9 enhances the stalk cell phenotype in a β_{IV}-spectrin–dependent manner, we next tested whether β_{IV}-spectrin mediates this effect by altering the downstream expression of key stalk cell genes. Specifically, we assessed for changes in ID1, ID3, and Hes1—all of which are known as direct transcriptional targets of the BMP9/Smad1/5 pathway critical for stalk cell specification during vascular sprouting (Itoh *et al.*, 2004; Peng *et al.*, 2004; Kobayashi and Kageyama, 2010; Kim *et al.*, 2012; Rostama *et al.*, 2015; Seong *et al.*, 2021). Surprisingly, BMP9 treatment resulted in robust Smad1/5 activation and downstream ID1/3 and Hes1 gene expression even upon loss of β_{IV}-spectrin (Figure 4B, graph), suggesting that β_{IV}-spectrin does not target the canonical stalk cell genes of the BMP9/Smad1 pathway.

But because the BMP9/Smad1 pathway coordinates with Notch signaling to further strengthen the stalk cell potential during vascular sprouting (Itoh *et al.*, 2004; Upton *et al.*, 2009; Moya *et al.*, 2012; Kerr *et al.*, 2015; Rochon *et al.*, 2015; Rostama *et al.*, 2015; Guihard *et al.*, 2020; Seong *et al.*, 2021), we next assessed for β_{IV}-spectrin–dependent changes in Notch-dependent markers. Interestingly, while BMP9 selectively enhanced the expression of stalk cell markers as expected in control cells (i.e., Jagged1 and Notch1) (Larrivée *et al.*, 2012; Chen *et al.*, 2019), β_{IV}-spectrin–depleted cells displayed low basal levels of the stalk cell markers and largely proved to be unresponsive to BMP9 treatment (Figure 4C, graphs). Instead, a significant up-regulation in tip cell markers was observed in β_{IV}–short hairpin RNA (shRNA) cells, thus indicating that β_{IV}-spectrin plays a critical role in the expression of Notch-dependent stalk cell markers. Moreover, because BMP9 was unable to promote the expression of Notch1 and Jagged1 despite the normal induction of ID1/3 and Hes1 (Figure 4, B and C, graphs), these findings suggested that the BMP9-induced β_{IV}-spectrin expression enhances stalk cell behavior through a signaling process distinct from the canonical ID1/3 and Hes1 pathway.

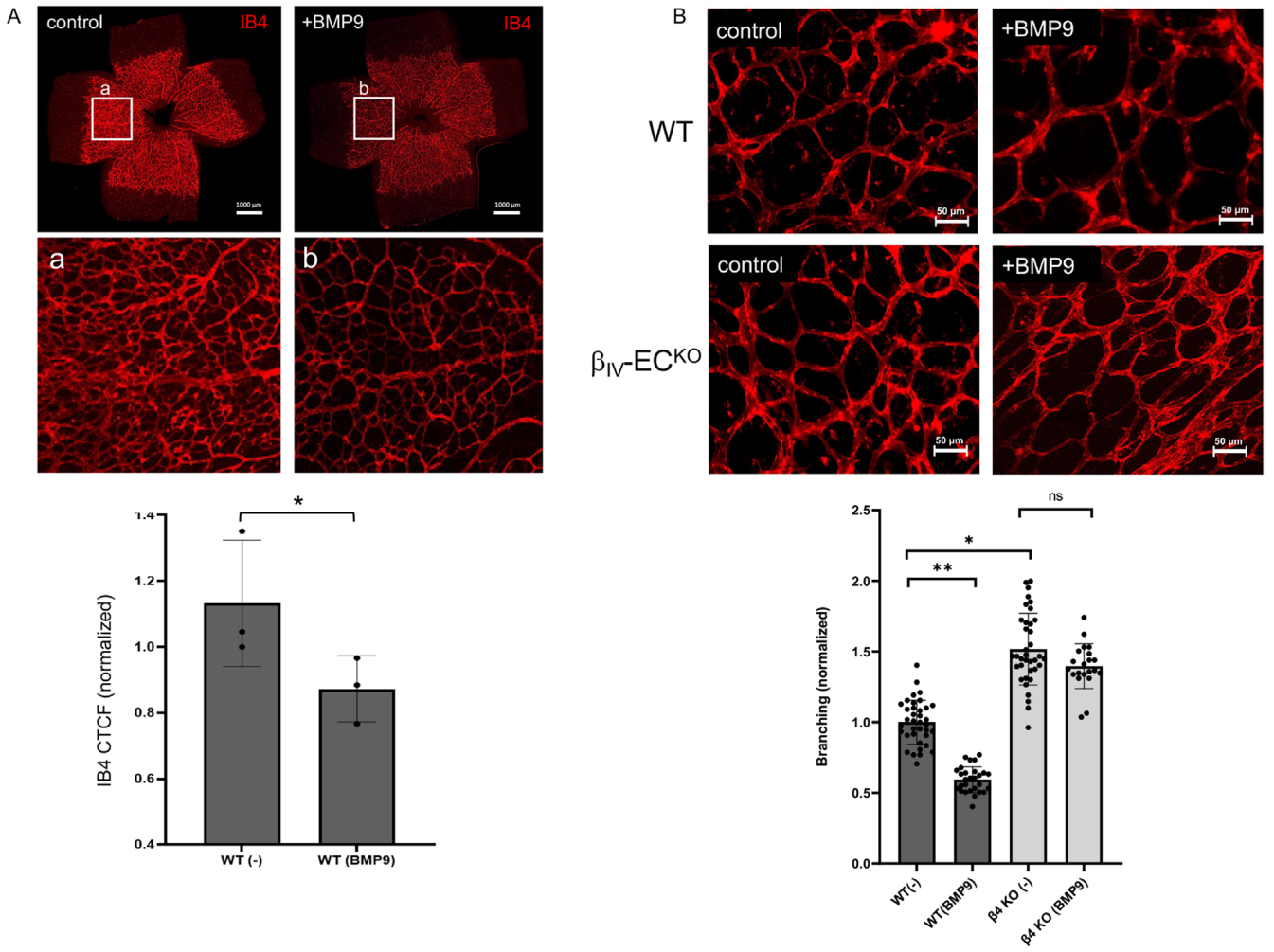

FIGURE 2: BMP9 regulation of angiogenesis requires β_{IV}-spectrin expression. (A) Representative immunofluorescence images of isolectin B4 (IB4) staining of P5 WT retinas in control (PBS) or upon BMP9 treatment (1 nM) via IP injection at P1 and P3. Inset images (a and b) demonstrate decrease in endothelial vessel branching upon BMP9 treatment. Graph quantification is based on average normalized CTCF values from three separate mice for both WT control and WT BMP9-treated retinas. Error bars indicate mean with SD, and the type 2 *t* test result shows $*p < 0.05$ relative to control (PBS). (B) Representative immunofluorescence images indicate isolectin B4 (IB4) staining of P5 WT and β_{IV}-EC^{KO} retina upon simultaneous tamoxifen induction and BMP9 treatment (1 nM) via IP injection at P1 and P3. Graph quantification indicates differences in endothelial vessel branching, where at least six regions of interest was measured in $n = 6$, 4, 5, and 4 separate mice for WT (control), WT BMP9 treatment, β_{IV}-EC^{KO} (control), and β_{IV}-EC^{KO} BMP9 treatment, respectively. Error bars indicate mean with SD, and the type 2 *t* test result shows $*p < 1E^{-10}$, $**p < 1E^{-15}$ relative to WT control (PBS). ns = nonsignificant.

BMP9 signaling regulates VEGFR2 expression and tip cell potential through the β_{IV}-spectrin/CaMKII complex

To identify the molecular mechanism controlled by BMP9-induced β_{IV}-spectrin gene expression, we performed a comparative quantitative proteomics analysis on control and β_{IV}-shRNA ECs upon BMP9 treatment. The proteomic heat map revealed 675 proteins that were statistically up-regulated in β_{IV}-spectrin–depleted cells while 585 were down-regulated (Figure 5A). The gene ontology analysis of these significant responders further indicated that the greatest fold enrichment occurred in biological processes related to EC migration and sprouting angiogenesis (Supplemental Figure S3, green dotted box), both of which were consistent with striking changes in tip cell characteristics. Indeed, further breakdown of these fold-enrichment clusters showed the presence of many prominent tip cell–specific markers including VEGFR2, the principal driver of vascular sprouting and tip cell specification (Figure 5B, red highlights). On the basis of these new data and our previous finding that β_{IV}-spectrin mediates VEGFR2 proteolysis (Kwak *et al.*, 2022), we hypothesized that BMP9 acts as a critical regulator of VEGFR2 turnover through increased β_{IV}-spectrin expression. Accordingly, results in control ECs showed a marked decrease in VEGFR2 over basal level upon BMP9 treatment, whereas in β_{IV}-shRNA cells the receptor level remained constant at two- to threefold higher than the control cells irrespective of the ligand (Figure 5C, top panel and graph). In contrast, VEGFR1, whose levels correlate with the stalk cell phenotype (Jakobsson *et al.*, 2010), remained at similar levels in both control and β_{IV}-shRNA cells (Figure 5C, second panel). Similarly, BMP9 treatment in vivo resulted in dramatically lower levels of VEGFR2, particularly along the radial front of sprouting retinal vessels in control mice, whereas the β_{IV}-EC^{KO} retinal vasculature displayed excessive VEGFR2 levels independent of ligand treatment (Figure 5D, graph). Therefore, while BMP9 is known to down-regulate VEGFR2 through Smad1/Hes1

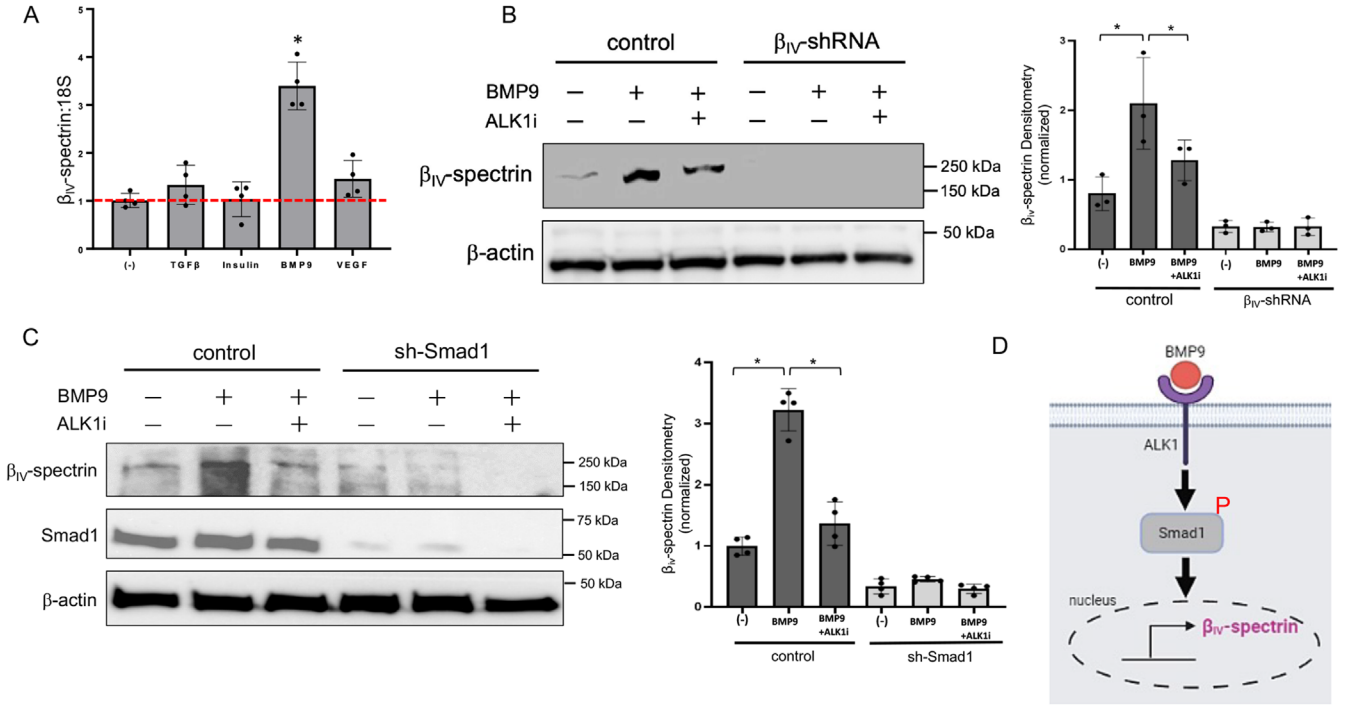

FIGURE 3: β_{IV}-Spectrin gene expression is mediated by the BMP9/ALK1/Smad1/5 pathway. (A) Quantification of β_{IV}-spectrin mRNA in MEECs by quantitative PCR analyzed by delta-delta-CT (ddCT) methods using 18S rRNA as internal control. MEECs were treated with TGF-β (200 pM), insulin (100 nM), BMP9 (1 nM), and VEGF (50 ng/ml) in serum-deprived media for 16 h followed by the qPCR experiment. Error bars indicate mean with SD, and the type 2 *t* test result shows $*p < 0.0001$ relative to control (no treatment). (B) Western blots show β_{IV}-spectrin levels in control MEECs and in sh-β_{IV}-spectrin stable cell lines treated with BMP9 (1 nM) alone or in the presence of ALK1 inhibitor (0.6 μM) in serum-starved condition for 16 h. Data are representative of three independent experiments. Fold change of β_{IV}-spectrin level relative to MEECs control (no treatment) is represented. Error bars indicate mean with SD, and the type 2 *t* test result shows $*p < 0.05$ compared with control or as indicated. (C) Western blots show β_{IV}-spectrin levels in control MEECs and in sh-Smad1 stable cell lines treated with BMP9 (1 nM) alone or in the presence of ALK1 inhibitor (0.6 μM) in serum-starved condition for 16 h. Data are representative of three independent experiments. Fold changes of β_{IV}-spectrin level relative to MEEC control (no treatment) are represented. Error bars indicate mean with SD, and the type 2 *t* test result shows $*p < 0.0005$ compared with control or as indicated. (D) Working model of BMP9 transcriptional activation of β_{IV}-spectrin through ALK1/Smad1 pathway. This schematic was created with BioRender.com.

gene regulation and Notch signaling cross-talk (Henderson *et al.*, 2001; Taylor *et al.*, 2002), here our data indicated that β_{IV}-spectrin is also a major transcriptional target in limiting VEGFR2 levels to maintain the proper tip/stalk cell balance during vascular sprouting.

We previously reported that β_{IV}-spectrin mediates VEGFR2 proteolysis by recruiting CaMKII to the plasma membrane, which then phosphorylates the receptor and promotes its internalization, ubiquitination, and degradation (Kwak *et al.*, 2022). We therefore first tested whether CaMKII is a key effector in BMP9-induced VEGFR2 turnover by using a CaMKII-selective inhibitor, KN93 (Wong *et al.*, 2019). In control ECs, BMP9 strongly down-regulated VEGFR2 expression, whereas cotreatment with KN93 strongly blocked this effect (Figure 6A). In contrast, β_{IV}-shRNA cells maintained high levels of VEGFR2 independent of BMP9 or KN93 treatment (Figure 6A, graph), suggesting that β_{IV}-spectrin is likely required for the local targeting of CaMKII to the membrane where it triggers the VEGFR2 phosphorylation–induced internalization and degradation. Next, we performed immunofluorescence studies in nonpermeabilized ECs to determine the cell surface levels of endogenous VEGFR2 upon treatment with BMP9 or KN93. Relative to control, BMP9 treatment caused a significant internalization of the receptor, whereas cotreatment with KN93 abrogated this effect (Figure 6B, inset panels and graph), thus indicating that BMP9 mediates VEGFR2 internalization through the β_{IV}-spectrin/CaMKII complex. Finally, we observed increased levels of VEGFR2 ubiquitination upon BMP9 treatment in control cells but not when cotreated with KN93, whereas β_{IV}-shRNA cells had little to no ubiquitination independent of ligand or CaMKII inhibition (Supplemental Figure S4). Overall, these findings support an essential role for BMP9 signaling in β_{IV}-spectrin/CaMKII–dependent VEGFR2 degradation that promotes Notch signaling and stalk cell specification during vascular sprouting.

DISCUSSION

BMP9 is considered a potent mediator of stalk cell differentiation during vascular sprouting as it drives the expression of many hallmark stalk cell genes, including ID1, ID3, and Hey1 through the ALK1/Smad1 pathway (Itoh *et al.*, 2004; Peng *et al.*, 2004; Upton *et al.*, 2009; Kobayashi and Kageyama, 2010; Kim *et al.*, 2012; Moya *et al.*, 2012; Seong *et al.*, 2021). While there is also mounting evidence of cross-talk between Smad and Notch signaling that further strengthens the stalk cell phenotype while suppressing the tip cell potential (Itoh *et al.*, 2004; Larrivée *et al.*, 2012; Aspalter *et al.*, 2015; Rostama *et al.*, 2015; Mouillesseaux *et al.*, 2016; Guihard *et al.*, 2020), our present work demonstrates that this cross-talk requires β_{IV}-spectrin, a new gene target of BMP9 signaling essential for sprouting angiogenesis and tip/stalk cell selection.

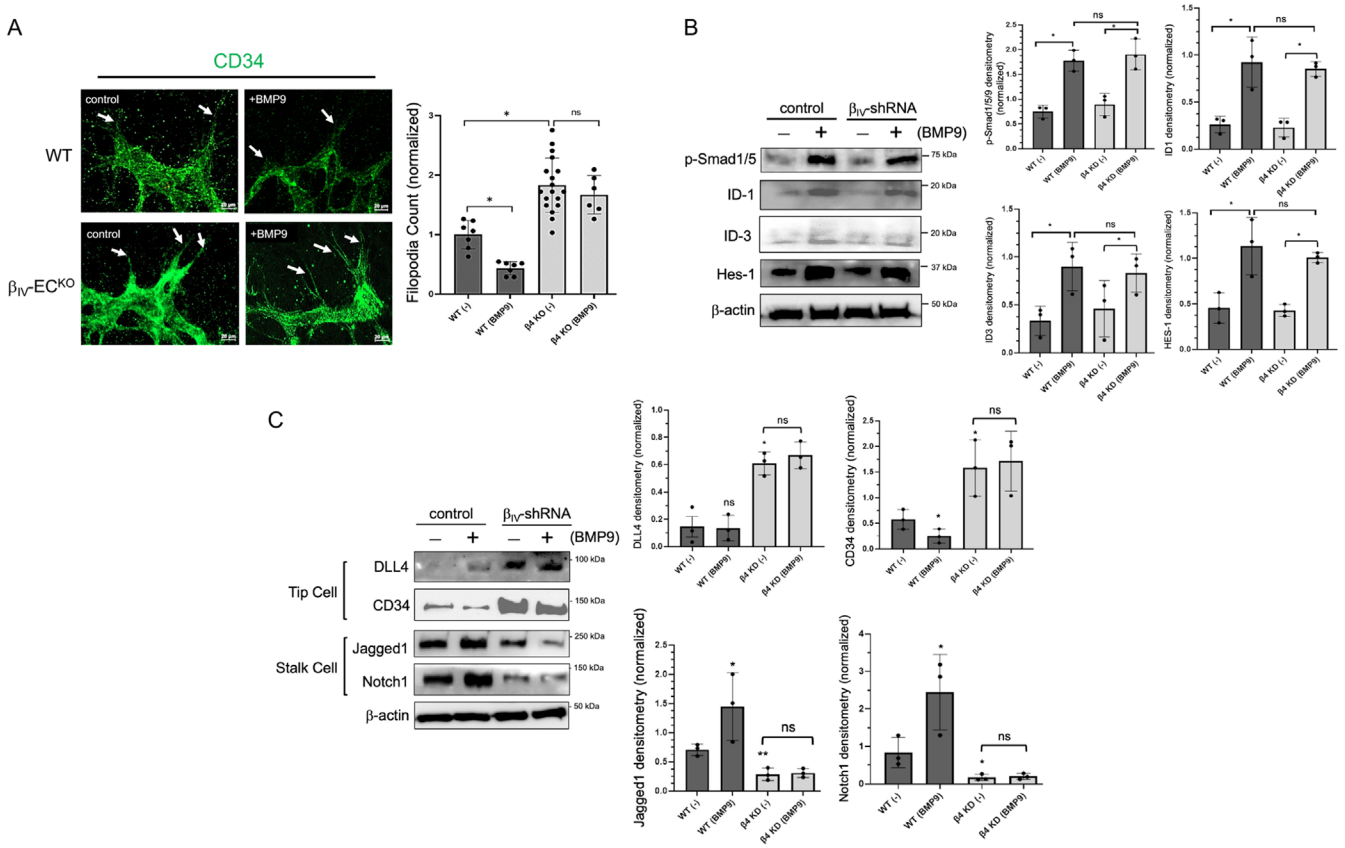

FIGURE 4: BMP9 regulation of the tip/stalk cell phenotypes requires β_{IV}-spectrin expression. (A) Magnification of CD34 fluorescence imaging show filopodial projections (white arrows) at the leading edge of the vascular plexus of WT and β_{IV}-EC^{KO} retinas at P5 upon simultaneous tamoxifen induction and BMP9 treatment (1 nM) via IP injection at P1 and P3. Graph represents percentage of filopodial counts from five separate mice for each group normalized to WT control (1 nM) retina. Error bars indicate mean with SD, and the type 2 *t* test result shows $*p < 1E^{-4}$ relative to WT control (PBS). ns = nonsignificant. (B) Western blot and densitometry quantifications show relative endogenous p-Smad 1/5, ID-1, ID-3, and Hes-1 levels in control MEECs and in sh-β_{IV}-spectrin stable cell lines upon BMP9 (1 nM) treatment in serum-starved condition for 16 h. Data are representative of three independent experiments. Error bars indicate mean with SD, and the type 2 *t* test result shows $*p < 0.05$ compared with control or as indicated. ns = nonsignificant. (C) Western blot and densitometry quantifications show relative endogenous DLL4, CD34, Jagged1, and Notch1 levels in control MEECs and in sh-β_{IV}-spectrin stable cell lines upon BMP9 (1 nM) treatment in serum-starved condition for 16 h. Data are representative of three independent experiments. Error bars indicate mean with SD, and the type 2 *t* test result shows $*p < 0.05$ compared with control. ns = nonsignificant.

The tip/stalk cell specification during vascular sprouting begins with increased VEGF signaling in tip cells that induces Dll4 up-regulation, which in turn activates Notch signaling in adjoining stalk cells to suppress the tip cell phenotype (Gerhardt *et al.*, 2003; Hellström *et al.*, 2007; Jakobsson *et al.*, 2010; Larrivée *et al.*, 2012; Moya *et al.*, 2012). Notably, this Notch activation is believed to play a key role in repressing the downstream VEGFR2 gene expression while enhancing VEGFR1 transcription (Hellström *et al.*, 2007; Larrivée *et al.*, 2012), although precisely how stalk cells initially enhance Notch expression to receive the Dll4 signal has remained unclear. Our data suggest that β_{IV}-spectrin is a critical determinant of Notch signaling during the early stages of stalk cell selection, as we observed that both Notch1 and Jagged1 are dramatically down-regulated upon loss of β_{IV}-spectrin expression. This effect appears to be largely independent of BMP9 signaling cross-talk with the downstream gene products such as ID1/3 and Hes-1, but rather through β_{IV}-spectrin–dependent turnover of the VEGFR2 receptor from the cell surface. This conclusion is consistent with the reciprocal relationship between VEGF/VEGFR2 signaling and Notch1 expression, which has been reported by others, and our own observation from cell-based and in vivo results.

Another conclusion from the present work relates to spectrin biology. Although many diverse functions have been defined for the different spectrin subunits over the years, their roles in the vascular system remain poorly characterized. In fact, there have been only two studies reported so far—one that implicates the role of α_{II}-spectrin in promoting angiogenesis at least in cell culture models (Machnicka *et al.*, 2020) and our recent work on the dynamic regulation of VEGFR2 signaling and vascular sprouting by β_{IV}-spectrin (Kwak *et al.*, 2022). Given that α_{II}-spectrin is more broadly expressed and capable of forming heterotetramers with other spectrin subunits, deciphering how α_{II}-spectrin and various other spectrin subunits coordinate with β_{IV}-spectrin in ECs will be a crucial next step in broadening our understanding of the elusive spectrin biology in the vascular system.

Finally, while the present study unveils how BMP9 controls the expression of β_{IV}-spectrin during angiogenesis, this circulating factor could potentially function in a similar manner in the nervous system

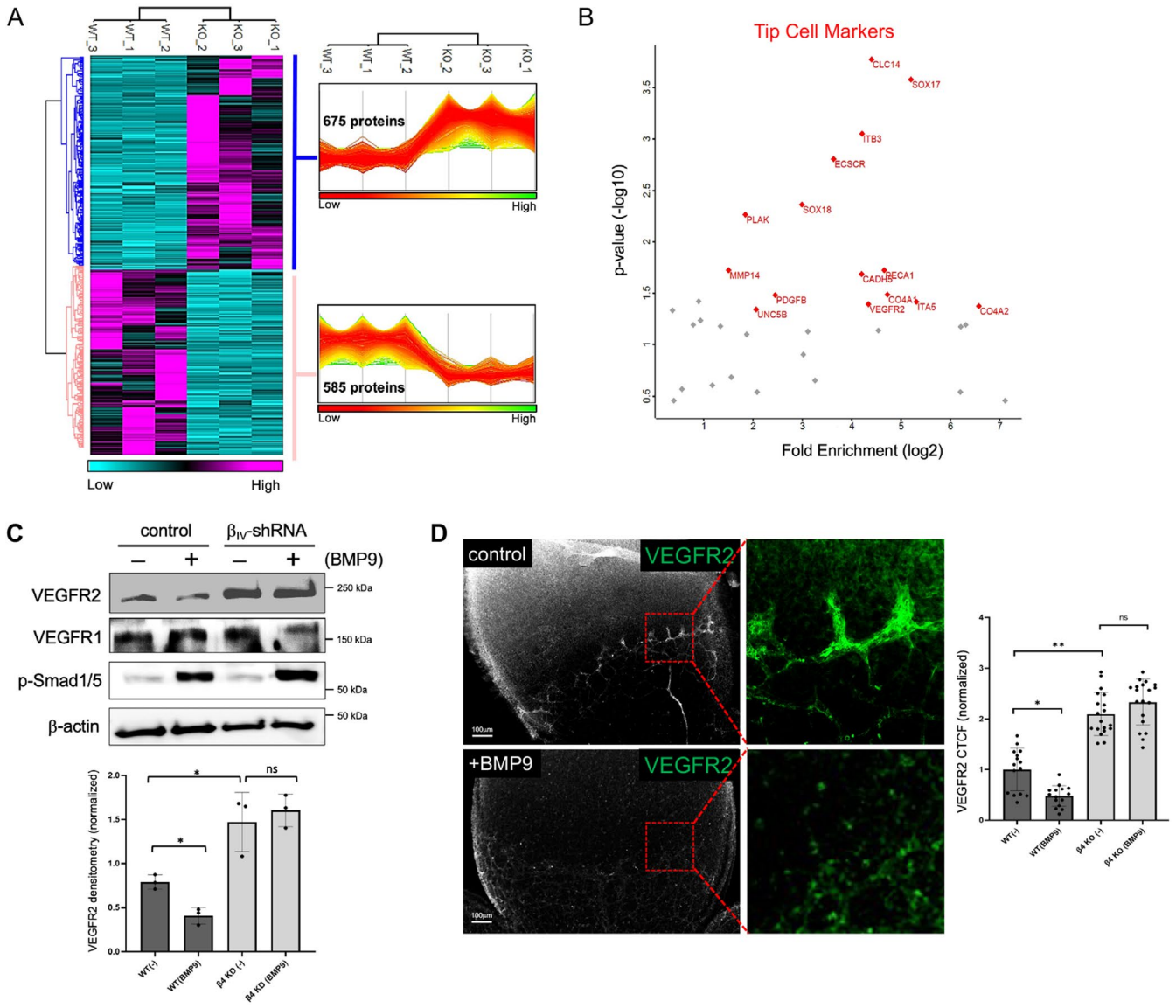

FIGURE 5: Comparative quantitative proteomics analysis identifies VEGFR2 as a key regulatory target of BMP9-induced β_{IV}-spectrin expression. (A) Unbiased hierarchical clustering of the 1260 significantly affected proteins confirmed that the expression patterns across the different individual biological samples cluster together accordingly as either control MEECs or sh-β_{IV}-spectrin cells upon BMP9 (1 nM) treatment. A heat map and linked dendrogram of the hierarchical clustering results provide a visual representation of the clustered matrix, and the associated profile plots further reveal consistency within groups of the corresponding protein expression patterns. (B) Scatter plot of the tip cell–associated markers identified in the quantitative MS-proteomics for control MEECs and sh-βIV-spectrin cells upon BMP9 (1 nM) treatment. (C) Western blot and densitometry quantifications show relative endogenous VEGFR2, VEGFR1, and p-Smad1/5 levels in control MEECs and in sh-βIV-spectrin stable cell lines upon BMP9 (1 nM) treatment in serum-starved condition for 16 h. Data are representative of three independent experiments. Error bars indicate mean with SD, and the type 2 *t* test result shows $*p < 0.05$ compared with control. ns = nonsignificant. (D) Representative immunofluorescence images indicate VEGFR2 level in the radial front of the P5 WT retinas upon BMP9 treatment (1 nM). Inset images (a and b) show decrease in VEGFR2 expression upon BMP9 treatment. Graph quantification is based on average normalized CTCF values from four separate mice for the indicated groups where at least three regions of interest were measured per group. Error bars indicate mean with SD, and the type 2 *t* test result shows $*p < 0.0005$, $**p < 2E^{-7}$ relative to control (PBS). ns = nonsignificant.

and heart. Along these lines, it is noteworthy that while BMP9 is released into circulation following its synthesis in the liver (Song *et al.*, 1995; Miller *et al.*, 2000), its close homologue, BMP10, is selectively expressed in cardiac tissues (Neuhaus *et al.*, 1999; Chen *et al.*, 2004; Nakano *et al.*, 2007). Therefore, future studies exploring the role of BMP9, BMP10, and other BMP members in β_{IV}-spectrin expression in various tissue types including, but not limited to, the nervous system, heart, and ECs may provide important and unexpected insights in many normal and pathophysiologic settings.

MATERIALS AND METHODS

Request a protocol through *Bio-protocol.*

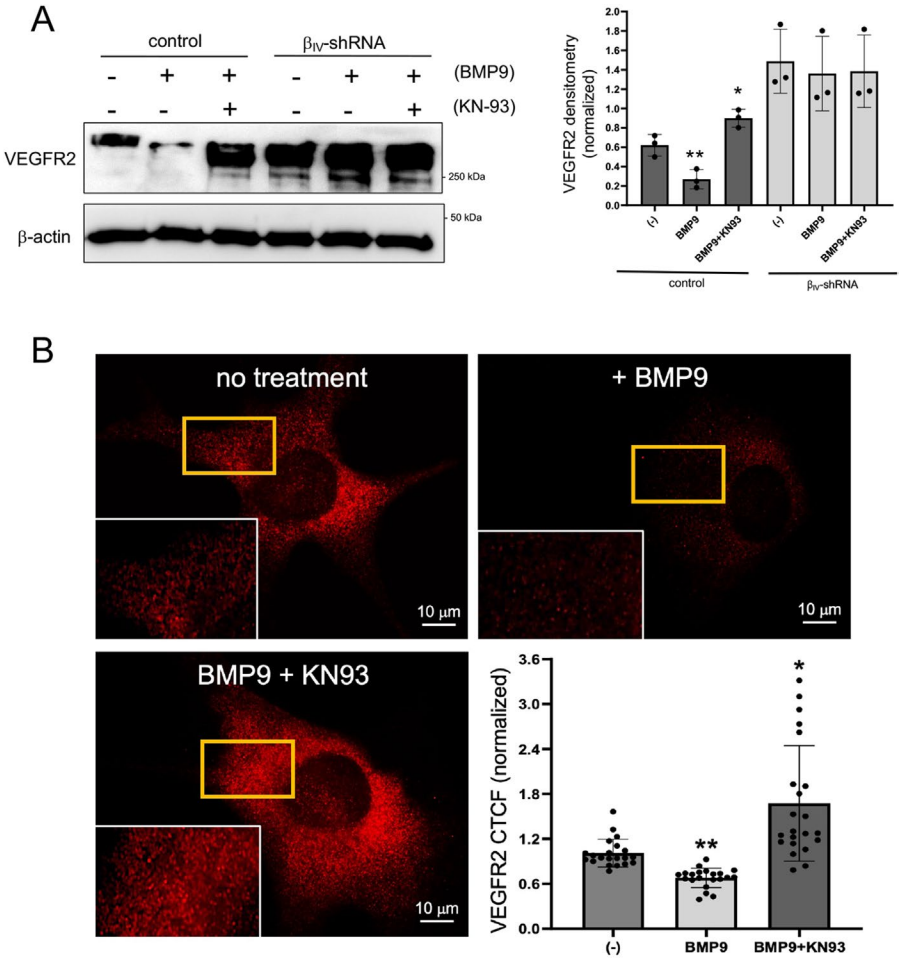

FIGURE 6: BMP9-induced VEGFR2 down-regulation is mediated by the β_{IV}-spectrin/CaMKII complex. (A) Western blot analysis shows VEGFR2 levels in control and β_{IV}-shRNA MEECs stable cell line upon treatment with BMP9 (1 nM) alone or with BMP9 (1 nM) and KN-93 (8 μM) for 16 h in serum-starved condition. Data are representative of three independent experiments. Error bars indicate mean with SD, and the type 2 *t* test result shows $*p < 0.03$, $**p < 0.01$ compared with control. (B) Representative immunofluorescence images indicate cell surface levels of endogenous VEGFR2 in nonpermeabilized control MEECs upon treatment with BMP9 (1 nM) alone or with BMP9 (1 nM) and KN-93 (8 μM) for 16 h in serum-starved condition. Graph quantification is based on average normalized CTCF value, where $n = 25$ cells. Error bars indicate mean with SD, and the type 2 *t* test result shows $*p < 0.005$, $**p < 3E^{-5}$ relative to control (no treatment).

β_{IV}-Spectrin knockout mice

β_{IV}-Spectrin fl/fl mice were derived from C57/Bl6 and were generous gifts from Thomas Hund (Ohio State University). An endothelial-specific Cre mouse model (Cdh5(PAC)-CreERT2) was purchased from Taconic. To generate and induce β_{IV}-spectrin knockout in $\beta_{IV}EC^{KO}$ mice, β_{IV}-spectrin fl/fl and Cdh5(PAC)-CreERT2 lines were first crossed and genotyped as described (Kwak *et al.*, 2022). All experiments were performed using male and female mice at age P5. All animal procedures were performed in accordance with the guidelines approved by the University of Arizona Institutional Animal Care and Use Committee.

Cell culture and transfection

MEECs were cultured in MCDB-131 (GIBCO) supplemented with 10% (vol/vol) fetal bovine serum, 2 mM L-glutamine (Life Technologies), 1 mM sodium pyruvate (Life Technologies), 100 μg/ml heparin (Sigma-Aldrich), and EC growth supplement (Sigma-Aldrich). Cells were maintained in T-75 culture flasks in a 37°C incubator with 5% CO_2 and were passaged every 2–3 d upon reaching 80–90% confluence.

β_{IV}-Spectrin and Smad1 knockdown stables cell line

The shRNA constructs for mouse β_{IV}-spectrin and Smad1 were purchased from Sigma-Aldrich. β_{IV}-spectrin knockdown (sh-β_{IV}-spectrin) was achieved by infecting β_{IV}-spectrin shRNA lentiviral particles into MEECs using 5 μg/ml Polybrene in regular growth media (Kwak *et al.*, 2022). Smad1 knockdown was generated by transfecting each mouse shRNA constructs into MEECs using Lipofectamine 2000. The shRNA targeting sequences for mouse Smad1 were as follows: 5′- TCCTATTTCATCCGTGTCTTA-3′ and 5′-TGGTGCTCTATTGTGTACTAT-3′ (Ahmed *et al.*, 2022). For both β_{IV}-spectrin and Smad1, stable knockdowns were achieved by selection with puromycin (5–10 μg/ml). Individual puromycin-resistant colonies were picked and scaled up as individual clones and were validated by Western blot comparing endogenous levels of β_{IV}-spectrin and Smad1 with that of scrambled control cells. Scramble control cells were transfected with scrambled control shRNA plasmid and were also selected with puromycin (5–10 μg/ml).

Real-time reverse transcriptase PCR

Total RNA was extracted from cells with Trizol reagent (Invitrogen), and 2 μg of RNA was converted to cDNA through the use of the High Capacity cDNA Reverse Transcription Kit (Applied Biosystems). β_{IV}-Spectrin was quantified by real-time reverse transcriptase PCR (Applied Biosystems) using SYBR green assay reagent and gene-specific primers (forward: 5-TCAGCATCCAAAGCAAACTG-3; reverse: 5-GCCACCTTGTGGTCAAATCT-3). Relative amplification was quantified by normalizing gene-specific amplification to that of 18S rRNA (5-GCTCTAGAATTACCACAGTTATC-3) and reverse (5-AAATCAGTTATGGTTCCTTTGGT-3) in each sample. Changes in mRNA abundance were calculated using the 2(–ΔΔCT) method. Quantitative PCR was run in triplicate. Statistical significance is presented as mean ± standard error (SE).

Immunofluorescence microscopy

Cells grown on coverslips were washed with phosphate-buffered saline (PBS), fixed with 4% paraformaldehyde, permeabilized in 0.1% Triton X-100/PBS for 5 min, and then blocked with 5% bovine serum albumin (BSA) in PBS containing 0.05% Triton X-100 for 1 h. Cells were incubated with appropriate primary and fluorophore-conjugated secondary antibodies for 2 h at room temperature (RT), washed, and then mounted with ProLong Antifade (Sigma). For measuring the cell surface level of VEGFR2, VEGFR2 was stained in nonpermeabilized cells, using PBS blocking solution without having Triton in it. Cells were incubated with VEGFR2 primary antibody and

fluorophore-conjugated secondary antibodies for 2 h at RT in the blocking buffer having no Triton, washed, and then mounted with ProLong Antifade (Sigma). Images were obtained via a Nikon A1R confocal microscope or Zeiss Axio7/Apatome2 inverted fluorescence microscope with a monochrome camera.

Isolation of retinas and immunofluorescence staining

Eyes were fixed for 15 min in 4% paraformaldehyde on ice and then rinsed twice with PBS. Upon fixing, the optic nerve and surrounding tissues were removed and the retinas were dissected with four radial incisions and then incubated in methanol at –20°C overnight. Methanol was rinsed out in PBS and then blocked (5% goat serum, 0.2% BSA, 0.3% Triton X-100 in 1× PBS) for 1 h at RT. Retinas were incubated with primary antibody in 100 µl of blocking solution at 4°C overnight and then washed for 15 min three times with 0.3% Triton X-100 in PBS. Retinas were incubated in secondary antibody at 4°C overnight and then washed four times for 30 min with 0.3% Triton X-100 in PBS. Retinas were mounted in anti-fade onto the cover slips and images acquired using a Nikon A1R confocal microscope or a Zeiss Axio7/Apatome2 inverted fluorescence microscope with a monochrome camera before analysis with the ImageJ/FIJI program.

Western blotting

Cell lysates were separated by SDS–PAGE and electrophoretic transferred onto PVDF (polyvinylidene difluoride) membranes (BIO-RAD). Transferred membranes were blocked with 5% skim milk in Tris buffered saline (TBS) with 0.1% Tween-20 and then incubated with primary antibodies at 4°C overnight. The following day, membranes were washed three times in TBS buffer with 0.1% Tween-20 and incubated with the secondary antibody for 45 min at RT. Membranes were washed five times in TBS buffer with 0.1% Tween-20 each 5 min and then imaging was done by the ChemiDoc Imaging system (BIO-RAD).

In-gel tryptic digestions, MS, database searching, and quantitative protoemics

In-gel tryptic digestion and high-performance liquid chromatography-electrospray ionization-MS/MS (tandem mass spectrometry having a single instrument with two mass analyzers) was performed exactly as previously described (Kruse *et al.*, 2017; Parker *et al.*, 2019). Tandem mass spectra were extracted from Xcalibur "RAW" files, and charge states were assigned with the ProteoWizard 3.0 msConvert script using the default parameters. The fragment mass spectra were searched against the Mus musculus SwissProt_2018_01 database (16,965 entries) with Mascot (Matrix Science; version 2.6.0) using the default probability cutoff score. The following search variables were used: 10 ppm mass tolerance for precursor ion masses and 0.5 Da for product ion masses; digestion with trypsin; a maximum of two missed tryptic cleavages; variable modifications of oxidation of methionine and phosphorylation of serine, threonine, and tyrosine. Cross-correlation of Mascot search results with X! Tandem was accomplished with Scaffold (version Scaffold_4.8.7; Proteome Software). Probability assessment of peptide assignments and protein identifications were made using Scaffold. Only peptides with ≥95% probability were considered. Progenesis QI for proteomics software (version 2.4; Nonlinear Dynamics Ltd) was used to perform ion intensity–based label-free quantification as previously described (Uhlorn *et al.*, 2021).

ACKNOWLEDGMENTS

We acknowledge the University of Arizona Cancer Center for assistance. This work was supported in part by National Institutes of Health grants GM148171 and CA275036 awarded to N.Y.L., University of Arizona Cancer Center internal funding, and a Cancer Center Support grant (P30 CA023074).

REFERENCES

Ahmed T, Flores PC, Pan CC, Ortiz HR, Lee YS, Langlais PR, Mythreye K, Lee NY (2022). EPDR1 is a noncanonical effector of insulin-mediated angiogenesis regulated by an endothelial-specific TGF-β receptor complex. J Biol Chem 298, 102297.

Aspalter IM, Gordon E, Dubrac A, Ragab A, Narloch J, Vizán P, Geudens I, Collins RT, Franco CA, Abrahams CL (2015). Alk1 and Alk5 inhibition by Nrp1 controls vascular sprouting downstream of Notch. Nat Commun 6, 7264.

Bennett V, Baines AJ (2001). Spectrin and ankyrin-based pathways: metazoan inventions for integrating cells into tissues. Physiol Rev 81, 1353–1392.

Bennett V, Lorenzo DN (2013). Spectrin- and ankyrin-based membrane domains and the evolution of vertebrates. Curr Top Membr 72, 1–37.

Bennett V, Lorenzo DN (2016). An adaptable spectrin/ankyrin-based mechanism for long-range organization of plasma membranes in vertebrate tissues. Curr Top Membr 77, 143–184.

Berghs S, Aggujaro D, Dirkx R Jr, Maksimova E, Stabach P, Hermel J-M, Zhang J-P, Philbrick W, Slepnev V, Ort T (2000). βIV spectrin, a new spectrin localized at axon initial segments and nodes of Ranvier in the central and peripheral nervous system. J Cell Biol 151, 985–1002.

Chen H, Shi S, Acosta L, Li W, Lu J, Bao S, Chen Z, Yang Z, Schneider MD, Chien KR, *et al.* (2004). BMP10 is essential for maintaining cardiac growth during murine cardiogenesis. Development 131, 2219–2231.

Chen W, Xia P, Wang H, Tu J, Liang X, Zhang X, Li L (2019). The endothelial tip-stalk cell selection and shuffling during angiogenesis. J Cell Commun Signal 13, 291–301.

Cianci CD, Zhang Z, Pradhan D, Morrow JS (1999). Brain and muscle express a unique alternative transcript of αII spectrin. Biochemistry 38, 15721–15730.

David L, Mallet C, Keramidas M, Lamandé N, Gasc J-M, Dupuis-Girod S, Plauchu H, Feige J-J, Bailly S (2008). Bone morphogenetic protein-9 is a circulating vascular quiescence factor. Circ Res 102, 914–922.

David L, Mallet C, Mazerbourg S, Feige JJ, Bailly S (2007). Identification of BMP9 and BMP10 as functional activators of the orphan activin receptor-like kinase 1 (ALK1) in endothelial cells. Blood 109, 1953–1961.

Desroches-Castan A, Tillet E, Bouvard C, Bailly S (2022). BMP9 and BMP10: Two close vascular quiescence partners that stand out. Dev Dyn 251, 158–177.

Djinovic-Carugo K, Gautel M, Ylänne J, Young P (2002). The spectrin repeat: a structural platform for cytoskeletal protein assemblies. FEBS Lett 513, 119–123.

Gaetani M, Mootien S, Harper S, Gallagher PG, Speicher DW (2008). Structural and functional effects of hereditary hemolytic anemia-associated point mutations in the alpha spectrin tetramer site. Blood 111, 5712–5720.

Gallagher PG, Maksimova Y, Lezon-Geyda K, Newburger PE, Medeiros D, Hanson RD, Rothman J, Israels S, Wall DA, Sidonio RF Jr, *et al.* (2019). Aberrant splicing contributes to severe alpha-spectrin-linked congenital hemolytic anemia. J Clin Invest 129, 2878–2887.

Gerhardt H, Golding M, Fruttiger M, Ruhrberg C, Lundkvist A, Abramsson A, Jeltsch M, Mitchell C, Alitalo K, Shima D (2003). VEGF guides angiogenic sprouting utilizing endothelial tip cell filopodia. J Cell Biol 161, 1163–1177.

Guihard PJ, Guo Y, Wu X, Zhang L, Yao J, Jumabay M, Yao Y, Garfinkel A, Boström KI (2020). Shaping waves of bone morphogenetic protein inhibition during vascular growth. Circ Res 127, 1288–1305.

Hellström M, Phng L-K, Hofmann JJ, Wallgard E, Coultas L, Lindblom P, Alva J, Nilsson A-K, Karlsson L, Gaiano N (2007). Dll4 signalling through Notch1 regulates formation of tip cells during angiogenesis. Nature 445, 776–780.

Hemmati-Brivanlou A, Thomsen GH (1995) Ventral mesodermal patterning in Xenopus embryos: expression patterns and activities of BMP-2 and BMP-4. Dev Genet 17, 78–89.

Henderson AM, Wang SJ, Taylor AC, Aitkenhead M, Hughes CC (2001). The basic helix-loop-helix transcription factor HESR1 regulates endothelial cell tube formation. J Biol Chem 276, 6169–6176.

Hund TJ, Koval OM, Li J, Wright PJ, Qian L, Snyder JS, Gudmundsson H, Kline CF, Davidson NP, Cardona N, *et al.* (2010). A β(IV)-spectrin/CaMKII signaling complex is essential for membrane excitability in mice. J Clin Invest 120, 3508–3519.

Itoh F, Itoh S, Goumans MJ, Valdimarsdottir G, Iso T, Dotto GP, Hamamori Y, Kedes L, Kato M, ten Dijke Pt P (2004). Synergy and antagonismbetween Notch and BMP receptor signaling pathways in endothelial cells. EMBO J 23, 541–551.

Jakobsson L, Franco CA, Bentley K, Collins RT, Ponsioen B, Aspalter IM, Rosewell I, Busse M, Thurston G, Medvinsky A, *et al.* (2010). Endothelial cells dynamically compete for the tip cell position during angiogenic sprouting. Nat Cell Biol 12, 943–953.

Kerr G, Sheldon H, Chaikuad A, Alfano I, von Delft F, Bullock AN, Harris AL (2015). A small molecule targeting ALK1 prevents Notch cooperativity and inhibits functional angiogenesis. Angiogenesis 18, 209–217.

Kim J-H, Peacock MR, George SC, Hughes CC (2012). BMP9 induces EphrinB2 expression in endothelial cells through an Alk1-BMPRII/ActRII-ID1/ID3-dependent pathway: implications for hereditary hemorrhagic telangiectasia type II. Angiogenesis 15, 497–509.

Kline CF, Wright PJ, Koval OM, Zmuda EJ, Johnson BL, Anderson ME, Hai T, Hund TJ, Mohler PJ (2013). βIV-Spectrin and CaMKII facilitate Kir6.2 regulation in pancreatic beta cells. Proc Natl Acad Sci USA 110, 17576–17581.

Knierim E, Gill E, Seifert F, Morales-Gonzalez S, Unudurthi SD, Hund TJ, Stenzel W, Schuelke M (2017). A recessive mutation in beta-IV-spectrin (SPTBN4) associates with congenital myopathy, neuropathy, and central deafness. Hum Genet 136, 903–910.

Kobayashi T, Kageyama R (2010). Hes1 regulates embryonic stem cell differentiation by suppressing Notch signaling. Genes Cells 15, 689–698.

Kobayashi T, Lyons KM, McMahon AP, Kronenberg HM (2005). BMP signaling stimulates cellular differentiation at multiple steps during cartilage development. Proc Natl Acad Sci 102, 18023–18027.

Kruse R, Krantz J, Barker N, Coletta RL, Rafikov R, Luo M, Hojlund K, Mandarino LJ, Langlais PR (2017). Characterization of the CLASP2 protein interaction network identifies SOGA1 as a microtubule-associated protein. Mol Cell Proteomics 16, 1718–1735.

Kwak E-A, Pan CC, Ramonett A, Kumar S, Cruz-Flores P, Ahmed T, Ortiz HR, Lochhead JJ, Ellis NA, Mouneimne G, *et al.* (2022). βIV-spectrin as a stalk cell-intrinsic regulator of VEGF signaling. Nat Commun 13, 1326.

Larrivée B, Prahst C, Gordon E, del Toro R, Mathivet T, Duarte A, Simons M, Eichmann A (2012). ALK1 signaling inhibits angiogenesis by cooperating with the Notch pathway. Dev Cell 22, 489–500.

Liu CH, Rasband MN (2019). Axonal spectrins: nanoscale organization, functional domains and spectrinopathies. Front Cell Neurosci 13, 234.

Machnicka B, Czogalla A, Hryniewicz-Jankowska A, Bogusławska DM, Grochowalska R, Heger E, Sikorski AF (2014). Spectrins: a structural platform for stabilization and activation of membrane channels, receptors and transporters. Biochim Biophys Acta 1838, 620–634.

Machnicka B, Ponceau A, Picot J, Colin Y, Lecomte MC (2020). Deficiency of αII-spectrin affects endothelial cell-matrix contact and migration leading to impairment of angiogenesis in vitro. Cell Mol Biol Lett 25, 3.

Miller AF, Harvey SA, Thies RS, Olson MS (2000). Bone morphogenetic protein-9: an autocrine/paracrine cytokine in the liver. J Biol Chem 275, 17937–17945.

Mouillesseaux KP, Wiley DS, Saunders LM, Wylie LA, Kushner EJ, Chong DC, Citrin KM, Barber AT, Park Y, Kim J-D (2016). Notch regulates BMP responsiveness and lateral branching in vessel networks via SMAD6. Nat Commun 7, 13247.

Moya IM, Umans L, Maas E, Pereira PN, Beets K, Francis A, Sents W, Robertson EJ, Mummery CL, Huylebroeck D (2012). Stalk cell phenotype depends on integration of Notch and Smad1/5 signaling cascades. Dev Cell 22, 501–514.

Nakano N, Hori H, Abe M, Shibata H, Arimura T, Sasaoka T, Sawabe M, Chida K, Arai T, Nakahara K-I (2007). Interaction of BMP10 with Tcap may modulate the course of hypertensive cardiac hypertrophy. Am J Physiol Heart Circ Physiol 293, H3396–H3403.

Neuhaus H, Rosen V, Thies RS (1999). Heart specific expression of mouse BMP-10 a novel member of the TGF-β superfamily. Mech Dev 80, 181–184.

Parker SS, Krantz J, Kwak EA, Barker NK, Deer CG, Lee NY, Mouneimne G, Langlais PR (2019). Insulin induces microtubule stabilization and regulates the microtubule plus-end tracking protein network in adipocytes. Mol Cell Proteomics 18, 1363–1381.

Peng Y, Kang Q, Luo Q, Jiang W, Si W, Liu BA, Luu HH, Park JK, Li X, Luo J (2004). Inhibitor of DNA binding/differentiation helix-loop-helix proteins mediate bone morphogenetic protein-induced osteoblast differentiation of mesenchymal stem cells. J Biol Chem 279, 32941–32949.

Ricard N, Ciais D, Levet S, Subileau M, Mallet C, Zimmers TA, Lee S-J, Bidart M, Feige J-J, Bailly S (2012). BMP9 and BMP10 are critical for postnatal retinal vascular remodeling. Blood 119, 6162–6171.

Rochon ER, Wright DS, Schubert MM, Roman BL (2015). Context-specific interactions between Notch and ALK1 cannot explain ALK1-associated arteriovenous malformations. Cardiovasc Res 107, 143–152.

Rostama B, Turner JE, Seavey GT, Norton CR, Gridley T, Vary CP, Liaw L (2015). DLL4/Notch1 and BMP9 interdependent signaling induces human endothelial cell quiescence via P27KIP1 and thrombospondin-1. Arterioscler Thromb Vasc Biol 35, 2626–2637.

Ruiz S, Zhao H, Chandakkar P, Chatterjee PK, Papoin J, Blanc L, Metz CN, Campagne F, Marambaud P (2016). A mouse model of hereditary hemorrhagic telangiectasia generated by transmammary-delivered immunoblocking of BMP9 and BMP10. Sci Rep 5, 37366.

Ruiz S, Zhao H, Chandakkar P, Papoin J, Choi H, Nomura-Kitabayashi A, Patel R, Gillen M, Diao L, Chatterjee PK, *et al.* (2020). Correcting Smad1/5/8, mTOR, and VEGFR2 treats pathology in hereditary hemorrhagic telangiectasia models. J Clin Invest 130, 942–957.

Scharpfenecker M, van Dinther M, Liu Z, van Bezooijen RL, Zhao Q, Pukac L, Lowik CW, ten Dijke P (2007). BMP-9 signals via ALK1 and inhibits bFGF-induced endothelial cell proliferation and VEGF-stimulated angiogenesis. J Cell Sci 120, 964–972.

Seong C-H, Chiba N, Kusuyama J, Subhan Amir M, Eiraku N, Yamashita S, Ohnishi T, Nakamura N, Matsuguchi T (2021). Bone morphogenetic protein 9 (BMP9) directly induces Notch effector molecule Hes1 through the SMAD signaling pathway in osteoblasts. FEBS Lett 595, 389–403.

Song JJ, Celeste AJ, Kong F-M, Jirtle RL, Rosen V, Thies RS (1995). Bone morphogenetic protein-9 binds to liver cells and stimulates proliferation. Endocrinology 136, 4293–4297.

Stewart A, Guan H, Yang K (2010). BMP-3 promotes mesenchymal stem cell proliferation through the TGF-β/activin signaling pathway. J Cell Physiol 223, 658–666.

Taylor KL, Henderson AM, Hughes CC (2002). Notch activation during endothelial cell network formation in vitro targets the basic HLH transcription factor HESR-1 and downregulates VEGFR-2/KDR expression. Microvasc Res 64, 372–383.

Tillet E, Bailly S (2015). Emerging roles of BMP9 and BMP10 in hereditary hemorrhagic telangiectasia. Front Genet 5, 456.

Uhlorn JA, Husband NA, Romero-Aleshire MJ, Moffett C, Lindsey ML, Langlais PR, Brooks HL (2021). CD4(+) T cell-specific proteomic pathways identified in progression of hypertension across postmenopausal transition. J Am Heart Assoc 10, e018038.

Upton PD, Davies RJ, Trembath RC, Morrell NW (2009). Bone morphogenetic protein (BMP) and activin type II receptors balance BMP9 signals mediated by activin receptor-like kinase-1 in human pulmonary artery endothelial cells. J Biol Chem 284, 15794–15804.

Urist MR (1965). Bone: formation by autoinduction. Science 150, 893–899.

Wang RN, Green J, Wang Z, Deng Y, Qiao M, Peabody M, Zhang Q, Ye J, Yan Z, Denduluri S, *et al.* (2014). Bone morphogenetic protein (BMP) signaling in development and human diseases. Genes Dis 1, 87–105.

Wong MH, Samal AB, Lee M, Vlach J, Novikov N, Niedziela-Majka A, Feng JY, Koltun DO, Brendza KM, Kwon HJ, *et al.* (2019). The KN-93 molecule inhibits calcium/calmodulin-dependent protein kinase II (CaMKII) activity by binding to Ca(2+)/CaM. J Mol Biol 431, 1440–1459.

Wozney JM, Rosen V, Celeste AJ, Mitsock LM, Whitters MJ, Kriz RW, Hewick RM, Wang EA (1988). Novel regulators of bone formation: molecular clones and activities. Science 242, 1528–1534.

Yang Y, Ogawa Y, Hedstrom KL, Rasband MN (2007). BetaIV spectrin is recruited to axon initial segments and nodes of Ranvier by ankyrinG. J Cell Biol 176, 509–519.

Yu PB, Deng DY, Lai CS, Hong CC, Cuny GD, Bouxsein ML, Hong DW, McManus PM, Katagiri T, Sachidanandan C, *et al.* (2008). BMP type I receptor inhibition reduces heterotopic [corrected] ossification. Nat Med 14, 1363–1369.